Journal of Solid State Chemistry 181 (2008) 2480–2487

Contents lists available at ScienceDirect

Journal of Solid State Chemistry

journal homepage: www.elsevier.com/locate/jssc

Structure, bonding and physical properties of tetragonal and orthorhombic SiS_2 from (hybrid) DFT calculations

Martijn A. Zwijnenburg [a,*], Robert G. Bell [b,a], Furio Corà [b,a,c]

[a] Davy Faraday Research Laboratory, University College London, Gower Street, Kathleen Lonsdale Building, 3rd Floor, London WC1E 6BT, UK
[b] Christopher Ingold Laboratories, Department of Chemistry, University College London, 20 Gordon Street, London WC1H 0AJ, UK
[c] Materials Simulation Laboratory, University College London, Gower Street, London WC1E 6BT, UK

ARTICLE INFO

Article history:
Received 14 March 2008
Received in revised form
19 May 2008
Accepted 2 June 2008
Available online 7 June 2008

Keywords:
Silicon sulphide
Chalcogenide
Silica
DFT

ABSTRACT

The energetics, structure and physical properties of tetragonal and orthorhombic SiS_2 were calculated by periodic density functional theory (DFT) calculations, using both localized orbital and projected augmented wave basis-sets. All methods applied agree upon the relative energies of the different polymorphs but show differences in the predicted geometries, which are minimized upon improving the basis-set quality. The hybrid PBE0 functional was found to give the best match between experimental and calculated structures. When comparing SiS_2 with its much better studied oxide analog silica, we observe that upon substituting sulphur for oxygen, the energy landscape changes dramatically. Other effects of changing S for O are found to be smaller Si–X–Si angles, a broader distribution of X–Si–X angles, a more flexible framework and a significantly reduced band gap. The latter is in line with the experimental observation of photoluminescence in related $GaGeS_2$ compounds and suggests that SiS_2 might find application in UV light emitting diodes. Finally, a comparison of the maximally localized Wannier functions demonstrates that the Si–S bonds in SiS_2 have a considerably more covalent character than the Si–O bonds in silica.

1. Introduction

Tetrahedral oxides (e.g. SiO_2, GeO_2, $Na_xSi_{1-x}Al_xO_2$) are among the most studied classes of materials due to their abundance in the Earth's crust and mantle, their technological importance in heterogeneous catalysis (support), and as an insulating layer in microelectronics. In contrast tetrahedral sulphides are much less well studied, with most theoretical attention focusing on amorphous SiS_2 and GeS_2 glasses [1–5]. Proposed applications for tetrahedral sulphides include optical amplifiers [6,7], inorganic photoresistors [8] and more recently crystalline nanoporous materials that combine porosity with (opto)electronic properties (luminescence, semiconduction) not found in their wide band gap oxide analogs [9]. Structurally, binary tetrahedral sulphides are also much richer than binary tetrahedral oxides. Where the latter predominantly form 3D materials built up from corner-sharing tetrahedra (with the exception of the reported synthesis and characterization in 1954 of the silica-W polymorph consisting of a packing of 1D chains [10]), tetrahedral sulphides crystallize in a range of 1D (chain), 2D (layers) and 3D crystal structures with both corner and edge-sharing tetrahedra.

SiS_2, even though of limited use for practical applications due to its sensitivity to oxygen and water [11,12], is the simplest model system of a tetrahedral sulphide and the subject of this paper. A search through the literature yields two experimental crystal structures. The most often studied polymorph is an orthorhombic structure corresponding to a packing of 1D chains of edge-sharing SiS_4 tetrahedra [13] (isostructural to silica-W, see Fig. 1), formed by a direct reaction between silicon and sulphur at high temperatures [11] or a reaction between silica and aluminium sulphide at high temperature [12,13]. This structure type is also found in heavier chalcogenides [13] ($SiSe_2$) and halides [14] ($BeCl_2$, $BeBr_2$ and BeI_2), where there are strong covalent bonds along the chain and dispersive interactions between the chains. The other crystal structure reported in the literature is a tetragonal SiS_2 compound formed by reacting silicon and sulphur at high temperature and pressure [15,16]. This structure (see Fig. 2) has the silicon atoms lying on a diamond net and is isostructural to silica and germania cristobalite. Physical data for SiS_2 crystalline compounds are limited to heat of formation [12], heat capacity at constant pressure [17], entropy [17] (all at 298.15 K) and the Raman spectra [12] of the orthorhombic structure. No experimental data for the relative thermodynamic stabilities of the polymorphs, their band gap and electronic structure is available.

* Corresponding author. Current address: Departament de Química Física and Institut de Recerca de Química Teòrica i Computacional, Universitat de Barcelona, Martí i Franquès 1, E-08028 Barcelona, Spain. Fax: +34 93 402 1231.
E-mail addresses: m.zwijnenburg@ucl.ac.uk, m.zwijnenburg@ub.edu (M.A. Zwijnenburg).

0022-4596/$ - see front matter © 2008 Elsevier Inc. All rights reserved.
doi:10.1016/j.jssc.2008.06.006

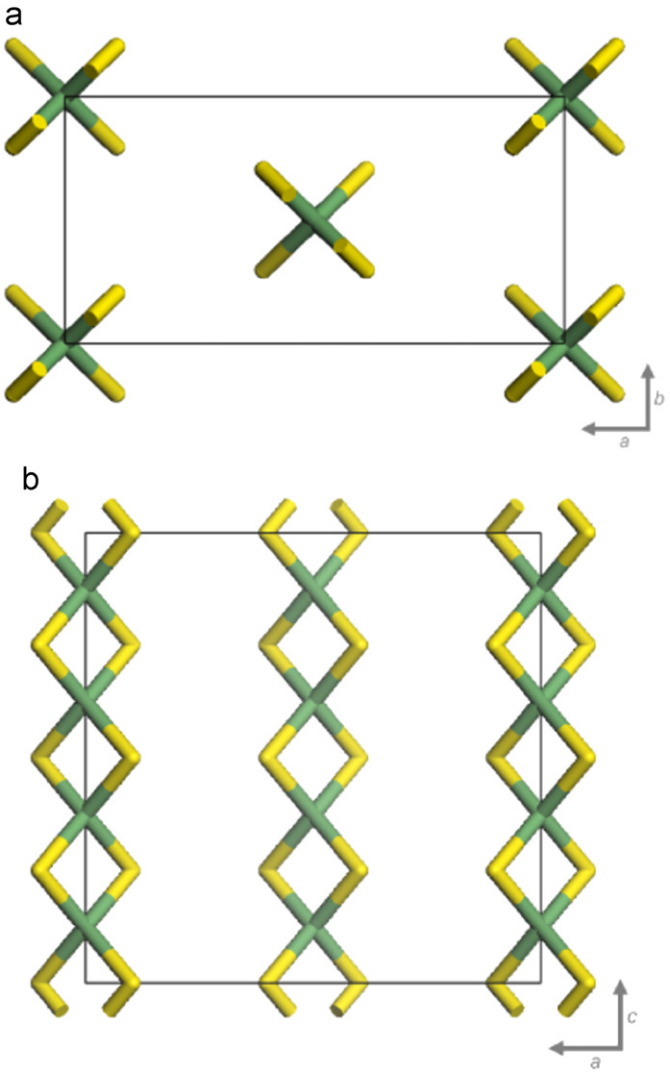

Fig. 1. Front and top-view of a unit-cell of orthorhombic SiS_2 clearly showing the 1D chains of edge shared SiS_4 tetrahedra (silicon atoms green, sulphur atoms green).

Here we use periodic density functional theory (DFT) calculations to evaluate the relative energies of the two experimentally synthesized silicon disulphide phases and estimate a selection of their physical properties, including infrared and Raman spectra, dielectric tensors and band gaps. Furthermore, we contrast the results obtained with those of their SiO_2 counterparts. To this end we also include in our study a sulphide version of the α-quartz structure, which is the most stable polymorph of silica at ambient pressure and temperature. The structures were optimized using both a GGA density functional and a hybrid version that included a fixed amount of Hartree–Fock exchange, and for all structures the gamma point phonons are calculated. The latter not only allow us to extract additional data but also to verify that all optimized structures are true minima with respect to the internal coordinates. This feature is important as for the SiS_2 quartz the absence of an experimental structure means that its starting structure could only be approximate and thus may optimize to *N*-order saddle points if left unchecked.

2. Computational methodology

The materials discussed in the paper have been investigated with periodic DFT calculations, employing the PBE [18] and hybrid

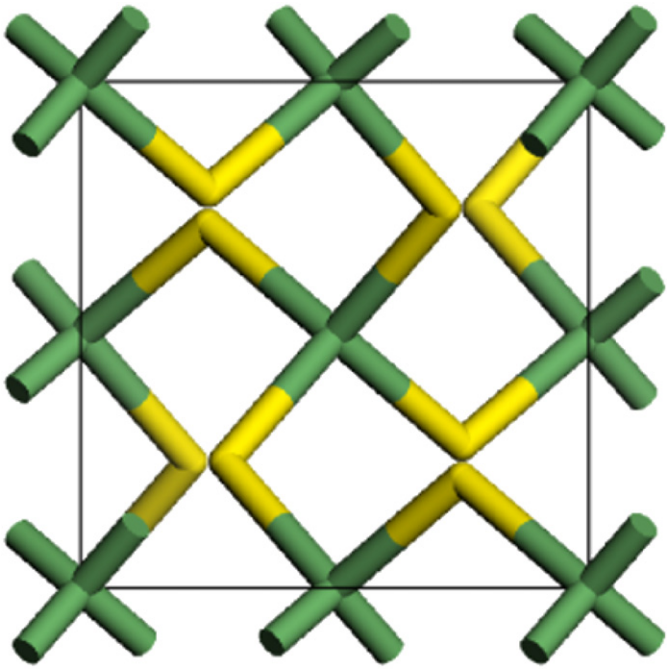

Fig. 2. Unit-cell of tetragonal SiS_2.

PBE0 [19] density functionals and localized Gaussian-type orbitals (PBE/LGTO and PBE0/LGTO, respectively) as implemented in the CRYSTAL06 [20] code. The basis-sets employed are expressed in a series of Gaussian-type functions and are generally of double valence plus polarization quality for each atomic species (Si and O [21], S [22]). The SiS_2 structures were additionally optimized with a modified Dunning's aug-cc-PVTZ basis-set [23] (in which the *s*, *p*, and *d* basis functions with exponent less than 0.1 and *f* basis functions with exponents less than 0.2 were removed to prevent linear dependency and SCF convergence problems), which corresponds to the practical basis-set limit. All elements are treated at the all-electron level.

We used a Monkhorst-Pack grid of $8 \times 8 \times 8$ and truncation thresholds of (7 7 7 7 14) for the Coulomb and exchange series [20], while SCF convergence thresholds were set to 1E-8 Hartree for both eigenvalues and total energies. These tolerances ensure high numerical accuracy in the calculations.

Geometry optimizations were restarted until the lattice parameters showed no further change and have been checked against the root-mean-square (RMS) and absolute value of the largest component for both gradients and nuclear displacements. Optimization was considered complete when the four conditions were simultaneously satisfied for both fractional coordinates and unit cell parameters, using the tight values of 1.2E-5 for the maximum gradient and 1.8E-5 for the maximum displacement (all in a.u.).

Gamma point phonons of the optimized structures were calculated using numerical differentiation of the analytical gradients of the energy with respect to the atomic displacements [24,25], where the second derivatives are calculated using a three-point formula and Cartesian displacements of 0.01 Å. To correct for LO–TO splitting due to long-range Coulomb effects, the dynamic dielectric tensor was evaluated by means of a finite field saw-tooth model as discussed in [26].

The basis-set superposition error (BSSE) was calculated using a counterpoise method for the optimized orthorhombic structure, using $2 \times 1 \times 1$ and $1 \times 2 \times 1$ super-cells in which all chains but one are removed in the *a* or *b* direction, respectively. The BSSE is then

the difference in total energy between a single point calculation where the relevant chains are removed and a single point calculation where the chains are removed but their basis-sets retained.

Some structures were also optimized using the PBE functional and the Projected Augmented Wave method [27,28] (PBE/PAW) as implemented in the VASP code [29]. All calculations employed a $4 \times 4 \times 4$ Monkhorst-Pack grid and a 900 eV energy cutoff, which was found to minimize the dependence of the basis-set quality on the cell-size and give well converged results. Final energies were obtained, after two subsequent restarts of the optimization cycle and a final single point calculation employing the tetrahedron method with Blöchl corrections.

3. Results and discussion

3.1. A structural and energetic properties

Table 1 gives the optimized geometry of the tetragonal SiS_2 structure and its energy difference with SiS_2 quartz as calculated with the different combinations of functional and basis-set. For comparison also the experimental geometry is shown. Both the PBE/LGTO and PBE0/LGTO structures are found to have larger lattice parameters than experiment; something that can also be observed for the *a* and *b* lattice parameters in the PBE/PAW optimised structure. The latter has a *c* lattice parameter that is much closer to the experimental value, though additional calculations show that elongation of the cell along the *c* direction is a very soft degree of freedom: deformation from the *c* lattice parameter obtained with PBE/PAW to the PBE/LGTO optimized value (while keeping *a* and *b* fixed) raises the energy by a mere 0.22 kJ/mol SiS_2, i.e. less than 1% of the energy difference between polymorphs. In such a flat potential energy surface (soft deformation mode), the equilibrium configuration is much more sensitive to the choice of computational parameters, even though computed energies are virtually unaffected. Moreover, improving the LGTO basis-set from double-zeta with polarization to triple-zeta with polarization and diffuse functions (the modified aug-cc-PVTZ basis, further referred to as LGTO(MTZ)) results in a PBE/LGTO *c* lattice parameter that is smaller and in line with the PBE/PAW prediction.

The best match between experimental and optimized structures is found for the PBE0/LGTO(MTZ) results. Comparing this with the PBE/PAW and PBE/LGTO(MTZ) optimized structures shows the importance of using a hybrid functional and bigger basis-sets than typically employed in the case of oxides for obtaining accurate geometries. Only the *a* lattice parameter remains larger than desired, which seems inherently linked to the larger than experimental Si–Si distances (and related Si–S–Si angle). In contrast, all methods (irrespectively of the basis-set employed) give very similar energy differences between tetragonal SiS_2 and SiS_2 quartz, with the former lying 32–35 kJ/mol SiS_2 below quartz at all levels of theory investigated, confirming the easier convergence of relative energies compared to geometries for these materials, and the small influence of the *c* lattice parameter on the energetics. The good agreement between the PAW and LGTO calculated energy differences between tetragonal SiS_2 and SiS_2 quartz further suggests that the BSSE in the LGTO calculated energies for the 3D structures is small (of the order of 1 kJ/mol SiS_2).

The orthorhombic structure proves to be a more difficult case, as the interactions holding the chains together include van der Waals forces, which are known to be poorly described by DFT. Furthermore, as these interactions are weaker than covalent bonds, BSSE is expected to have a more prominent effect. Table 2 gives a comparison of the experimental structure with the results of PBE/PAW, PBE/LGTO, PBE/LGTO(MTZ), PBE0/LGTO and PBE0/LGTO(MTZ) optimizations. While the *c* lattice parameter, which lies along the chain direction, and the intra-chain geometric parameters are in all cases well represented, the inter-chain distances and the related *a* and *b* lattice parameters are more poorly described, with differences of up to 18%. In the PBE/PAW calculation both *a* and *b* are overestimated by over 10%, while in the LGTO optimizations only the *a* lattice parameter is severely off. This asymmetry between the PAW and LGTO optimizations is the direct result of BSSE. For all structures (both optimized and experimental), the inter-chain distances in the *b* direction are smaller than those along *a*, leading to larger overlap between the basis-sets of atoms in different chains in the *b* direction and an increased BSSE. This BSSE artificially stabilizes contraction along the *b* direction thereby recovering the *b* lattice parameter in the LGTO optimizations by cancellation of errors. Quantitatively this is confirmed by explicit estimates of the BSSE, which is higher in the *b* direction (2.6 kJ/mol SiS_2 for PBE/LGTO) than in the *a* direction (1.3 kJ/mol SiS_2 for PBE/LGTO). The energy of a structure with the *a* and *b* lattice parameters from the PBE/PAW optimization and the *c* lattice parameter from the PBE/LGTO optimization lies only 1.1 kJ/mol SiS_2 higher and has a 0.2 kJ/mol SiS_2 lower BSSE; this finding confirms that the *b* (and *a*) lattice parameters in orthorhombic SiS_2 are soft degrees of freedom, and the true PBE (BSSE free) minimum indeed lies at a larger *b*. This observation is further supported by the fact that the PBE/LGTO(MTZ) optimized structure has a *b* lattice parameter that lies closer to that in the PBE/PAW optimized structure and smaller BSSE values (1.8 and 1.0 kJ/mol SiS_2 in the *b* and *a* direction, respectively). The best match with the experimentally determined structure is once more obtained using the combination of PBE0 functional and LGTO(MTZ) basis-set.

The energy differences of orthorhombic SiS_2 with respect to SiS_2 quartz are also reported in Table 2. All five methods employed yield consistent results, with orthorhombic SiS_2 lying 43–49 kJ/mol

Table 1
Comparison of the experimental and DFT optimized structures for the tetragonal SiS_2 structure and its energy difference with the quartz structure (all distances in Å, all angles in degrees and the energy difference in kJ/mol SiS_2)

	Experiment	PBE/LGTO	PBE/LGTO(MTZ)	PBE/PAW	PBE0/LGTO	PBE0/LGTO(MTZ)
a	5.420	5.656	5.668	5.644	5.581	5.591
c	8.718	8.849	8.768	8.717	8.820	8.733
Si–S	2.13	2.17	2.16	2.15	2.15	2.14
S–S	3.38	3.45	3.43	3.41	3.42	3.40
S–S	3.66	3.75	3.73	3.74	3.71	3.69
Si–Si	3.47	3.59	3.58	3.57	3.56	3.55
Si–S–Si	109.4	111.5	111.7	111.9	111.5	111.6
S–Si–S	105.2	105.0	104.9	104.9	105.2	105.0
S–Si–S	118.5	118.8	119.2	119.2	118.3	118.8
ΔE_{T-Q}	–	−32	−33	−33	−33	−35

Table 2
Comparison of the experimental and DFT optimized structures for the orthorhombic SiS_2 structure and its energy difference with the SiS2 quartz structure (all distances in Å, all angles in degrees and the energy difference in kJ/mol SiS_2)

	Experiment	PBE/LGTO	PBE/LGTO(MTZ)	PBE/PAW	PBE0/LGTO	PBE0/LGTO(MTZ)
a	9.543	11.680	11.437	11.199	11.318	11.178
b	5.564	5.633	6.011	6.363	5.598	5.941
c	5.552	5.629	5.624	5.629	5.594	5.591
Si–S	2.13	2.17	2.16	2.15	2.15	2.14
S–S	3.24	3.29	3.28	3.26	3.25	3.24
Si–Si	2.78	2.81	2.81	2.79	2.80	2.80
Si–S–Si	81.2	81.1	81.3	81.2	81.4	81.6
S–Si–S	98.8	98.9	98.7	98.8	98.6	98.4
S–Si–S	114.0	113.6	114.9	115.0	114.3	115.1
S–Si–S	116.1	116.4	115.3	115.1	116.0	115.4
ΔE_{R-Q}	–	−43	−45	−47	−48	−49

SiS_2 below quartz. Taking into account the small size of the BSSE compared with these energy differences and the weak nature of the van der Waals forces between the chains, their effect on the size of these energy differences is expected to be small. The latter finding is supported by a constrained PBE0/LGTO optimization on an isolated chain (*a* and *b* both set to 100 Å), which by construction has no inter-chain BSSE and no van der Waals contribution to the total energy, and still lies 41 kJ/mol SiS_2 below quartz-structured SiS_2 and 8 kJ/mol below the tetragonal polymorph.

When comparing the energy landscape of SiS_2 with that of SiO_2 as determined experimentally [30] and computationally [31–35], it is clear they differ dramatically (as previously observed by us in a more limited study focusing on nanoporous SiS_2 structures employing only the LGTO approach [36]). Whereas quartz is the lowest energy structure for SiO_2, it lies highest in energy among the three SiS_2 structures considered here. Cristobalite (i.e. the tetragonal SiS_2 structure) lies in its silica form slightly above quartz topology while as sulphide it is considerably stabilized compared with the quartz structure. The biggest difference, however, is observed for the chain structure (orthorhombic SiS_2). While its silica form (silica-W) has been calculated to lie approximately 120 kJ/mol SiO_2 above quartz by, respectively Hamann [37,38] and Wojdel et al. [39] using a range of different methods, we predict its sulphide version to lie 41–49 kJ/mol SiS_2 below quartz. This change in energy landscape is accompanied by an overall decrease in the size of the Si–X–Si angles and more extreme X–Si–X angles when substituting S for O.

The calculated thermodynamic stability of orthorhombic SiS_2 is in line with its facile synthesis and the fact that it can be purified by sublimation [12], and suggests that the appearance of non-3D structures for SiS_2 is due to the thermodynamic stabilization of their typical structural motifs, i.e. the edge-sharing of tetrahedra. A similar trend is also expected to happen in the case of heavier chalcogenides, and could make them ideal building materials for low-dimensional nanostructures [40,41].

We observed previously that the SiX_4 tetrahedra in SiS_2 and GeS_2 quartz are considerably more distorted than in their oxide analogs and proposed a simple model which relates this increased flexibility to the lower electrostatic cost of tetrahedral distortion in sulphides [42]. While this explains the tolerance of SiS_2 for the more extreme X–Si–X angles observed in both edge and corner-sharing structures, it does not provide an explanation for the energetic preference of SiS_2 for edge-sharing tetrahedra. However, our calculated data support an inverse correlation between Si–S–Si angles and thermodynamic stability of SiS_2 materials (i.e. the smaller the Si–S–Si angle the lower a material lies in energy), which is consistent with the smaller Si–S–Si angles required for edge-sharing among tetrahedra, and the high occurrence of edge-sharing among binary compounds of heavy chalcogenides and halides.

Table 3
PBE0/LGTO calculated static (ε_0) and dynamic (ε_∞) dielectric tensor diagonal elements for tetragonal and orthorhombic SiS_2

	Direction	ε_0	ε_∞
Tetragonal SiS_2	*x*	6.13	4.38
	z	6.81	4.23
Orthorhombic SiS_2	*x*	2.69	2.54
	y	2.73	2.54
	z	5.59	3.35

3.2. Dielectric and vibrational properties

Table 3 gives the PBE0/LGTO estimates of the static and dynamic dielectric tensors for tetragonal and orthorhombic SiS_2. Overall, the values calculated for SiS_2 are considerably larger than those found for silica materials [25], suggesting that the (valence) electrons in the sulphide are more polarisable than in the oxide. Moreover, the values for orthorhombic SiS_2 clearly reflect the anisotropy of the underlying structure, with the dielectric tensor components in the inter-chain directions being considerably smaller than along the intra-chain direction. Electrostatic coupling between the different chains appears to be very weak, and the electronic polarisability has a preferential orientation along the Si–S bonds.

Table 4 gives the calculated PBE0/LGTO infrared and Raman frequencies (including intensities in the former case) for the tetragonal and orthorhombic SiS_2 structures. The infrared spectra (as judged from the infrared active TO-modes observed in a typical infrared experiment) are dominated by a very strong peak at 511 and 485 cm^{-1}, respectively; the presence of two peaks at higher frequency in the case of orthorhombic SiS_2 and several of lower frequency for tetragonal SiS_2 allows for easy experimental discrimination. Even in the absence of intensities there is a reasonable match between the experimentally measured [12] (powder) and calculated Raman spectra for orthorhombic SiS_2, with a maximum deviation of 14 cm^{-1} for the highest frequency mode at 626 cm^{-1}. This good agreement is customary for hybrid functionals with a percentage of HF in the range of 20–25%, such as PBE0 and B3LYP. The calculated Raman spectra for tetragonal SiS_2 are considerably different, facilitating the analytical use of Raman to discriminate among possible SiS_2 structures. Especially, the B1G Raman active mode at 640 cm^{-1} (experimentally at 626 cm^{-1}), which corresponds to a breathing mode of the 2-ring, seems to be a clear fingerprint of the presence of Si_2S_2 2-rings (and thus edge-sharing tetrahedra) in SiS_2 materials.

Table 4
Comparison of the infrared and Raman active modes of orthorhombic and tetragonal SiS_2 (all frequencies in cm^{-1}, LO modes in italics, intensities were available in brackets)

υ_{IR} Tet (PBE0/LGTO)	υ_{IR} Ortho (PBE0/LGTO)	υ_{Raman} Tet (PBE0/LGTO)	υ_{Raman} Ortho (PBE0/LGTO)	υ_{Raman} Ortho (EXP[12])
122 (29)	191 (5)	122	64	
213 (157)	191 (2)	213	143	
252 (35)	485 (1698)	252	181	
476 (809)	596 (198)	295	187	185
511 (1564)	608 (179)	318	363	352
553 (323)		476	443	
		496	445	433
		511	450	
		553	640	626
126 (16)	*192 (4)*	*126*		
235 (78)	*610 (1698)*	*235*		
254 (19)	*624 (199)*	*254*		
541 (16)		*541*		
548 (888)		*548*		
594 (1755)		*594*		

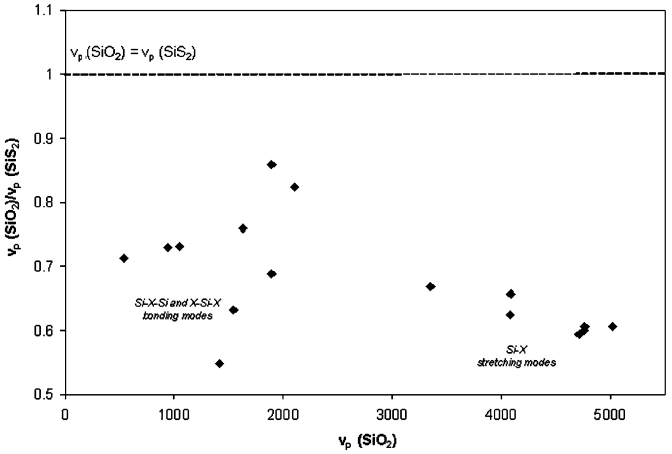

Fig. 3. Ratio of SiS_2 and SiO_2 pseudo-frequencies (all atomic masses set to equal (1) calculated for the quartz structure, plotted against the pseudo-frequencies for the SiO_2 structure.

To complete the comparison of SiO_2 and SiS_2, we have also calculated a set of pseudo-frequencies of SiO_2 and SiS_2 quartz, obtained by setting all the isotope masses equal to unity (as previously reported by us in Ref. [36]). The ratio of the SiS_2 and SiO_2 pseudo-frequencies is plotted against the silica pseudo-frequencies in Fig. 3; depending on the particular mode, the ratio is 0.9–0.5 or in other words the pseudo-frequencies are 10–50% lower in the case of SiS_2 than for SiO_2 quartz. The calculated red shift is strongest in the high-frequency modes with a large Si–X stretching component and the intermediate frequency X–Si–X and Si–X–Si bending modes, but is expected to be still sizeable for the low-frequency rigid unit modes [43] that are responsible for the materials' macroscopic flexibility. The lowering of the pseudo-frequencies indicates a similar decrease in the generalized force constants for SiS_2. The red shift is thus clear proof that substitution of oxygen by sulphur leads not only to a change in the energy landscape but also to an increase in the material's flexibility (and thus a decrease in the energetic cost of distorting the X–Si–X and Si–X–Si angles), while its origin must be sought (at least for inter-tetrahedral distortions involving Si–X–Si angles) in a change in the ionicity of the material [42].

3.3. Electronic and optical properties

The PBE0/LGTO Kohn-Sham band gap, which is expected to be a good approximation to the true valence many-body band gap

Table 5
Calculated PBE0/LO Kohn–Sham band-gap and energy gap between the conduction and valence band at the Γ point for the different SiS_2 and SiO_2 structures examined

	Band-gap (eV)	Γ-gap (eV)
Tetragonal SiS_2	5.22(5.06)	5.37(5.15)
Orthorhombic SiS_2	5.05(5.02)	6.27(6.22)
SiS_2 quartz	4.38	4.88
SiO_2 cristobalite	8.66	8.66
SiO_2 quartz	8.63	8.90

PBE0/LGTO(MTZ) calculated values, where available, are given in brackets.

[44], was calculated for the three sulphide and two silica structures examined in this paper, and found to lie between 4.4 and 5.2 eV and around 8.6 eV, respectively (see Table 5). Increasing the basis-set in case of the sulphides (PBE/LGTO(MTZ) for both geometry optimization and band structure) leads to a minor shift in the calculated band gaps of less than 0.05 eV for orthorhombic SiS_2 and less than 0.2 eV for tetragonal SiS_2. The slightly larger variation in the latter case is most likely caused by its greater geometric relaxation when increasing the basis-set for tetragonal SiS_2. Substitution of oxygen by sulphur thus leads to a considerable decrease in the band gap, with the system moving from a wide gap insulator towards a semiconductor. There are no experimental measurements available for the band gap in (crystalline) SiS_2. However, the calculated gap reduction is in line with experimental observation for glassy GeS_2 compared with GeO_2 [45] and the recent observation of photoluminescence for $Ga_xGe_{(1-x)}S_2$-TAEA (where TAEA is an organic cation) and related materials [9].

All SiS_2 structures are found to have indirect band gaps, even tetragonal SiS_2 whose SiO_2 analog has a direct band gap (see Fig. 4). However, analysis of the band structure of tetragonal SiS_2 in Fig. 5 shows that the bottom of the conduction band lies at the Γ-point while the top of the valence band is composed of levels with very small dispersion in reciprocal space (considerably less than for SiO_2 cristobalite). The difference between the band gap and the energy gap between the conduction and valence bands at the Γ-point is very small (less than 0.2 eV) and the material can therefore be argued to behave as having a direct band gap. Tetragonal SiS_2 thus might be able to absorb or spontaneously emit near ultraviolet light, and find application in devices such as ultraviolet light emitting diodes. Compared with AlN and AlGaN alloys that have a similar band gap [46], tetragonal SiS_2 has a much lower density and a more open structure. One can speculate that hypothetical zeolite-like SiS_2 structures [36] might

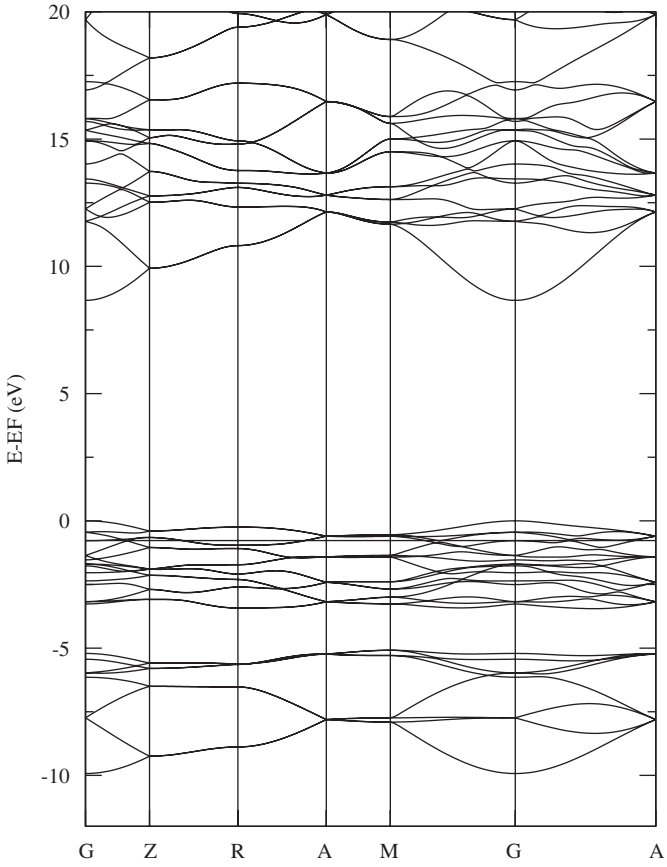

Fig. 4. Calculated PBE0/LGTO band structure of SiO_2 cristobalite.

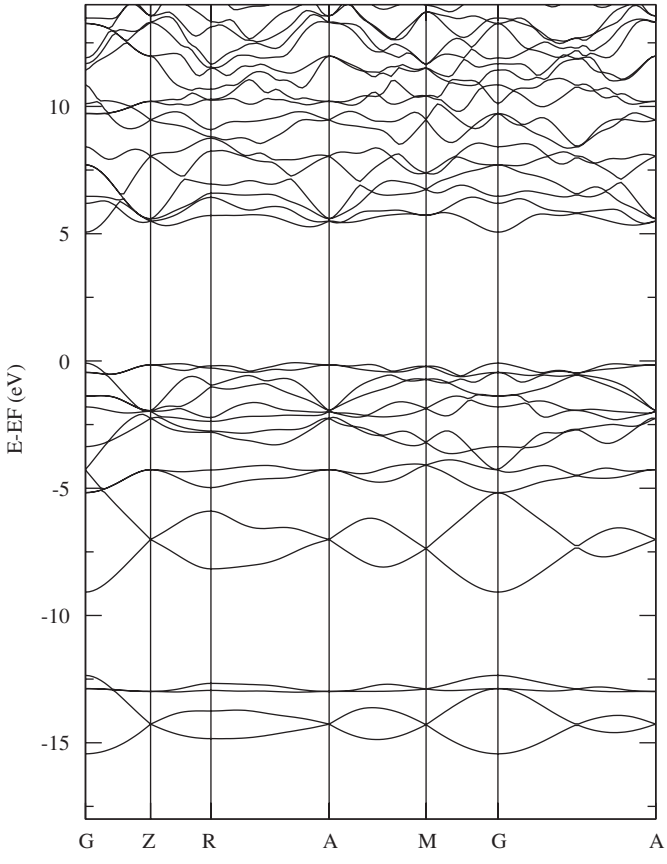

Fig. 5. Calculated PBE0/LGTO(MTZ) band structure of tetragonal SiS_2.

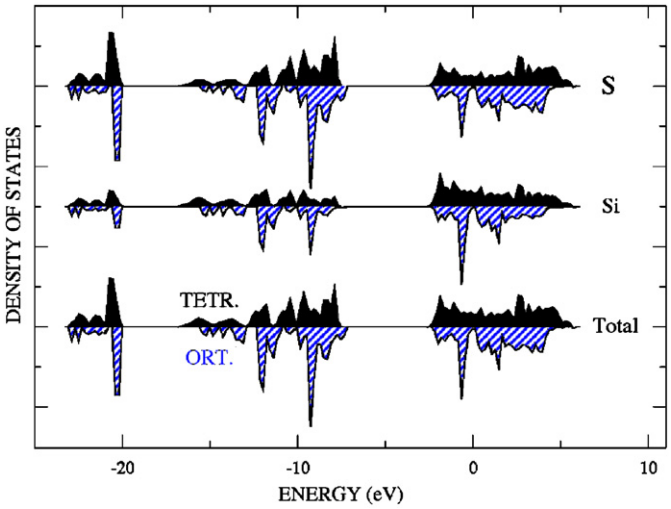

Fig. 6. Calculated PBE0/LGTO(MTZ) density of states of tetragonal and orthorhombic SiS_2. We report separately the total DOS and its projections onto the basis sets of Si and S atoms.

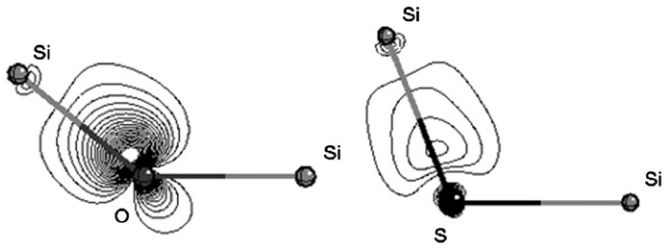

Fig. 7. Plots of the localized Wannier functions corresponding to the valence orbitals for SiO_2 (left) and SiS_2 (right) versions of the diamond structure.

even combine porosity on a molecular scale with the absorption or emission of near ultraviolet light, and have the potential for novel multifunctional applications.

Fig. 6 shows the calculated total and projected density of states (DOS) for tetragonal and orthorhombic SiS_2. Overall the two DOS look very similar, except for the fact that the bands in orthorhombic SiS_2 are sharper. The latter is a direct result of the reduced dimensionality of the bonded electron system in orthorhombic SiS_2 (1D compared with 3D in the tetragonal polymorph). The top of the valence band for both tetragonal and orthorhombic SiS_2 is found to consist of non-bonding sulphur (3*p*) states, while the bottom of the conduction band is found to consist predominantly of anti-bonding states between sulphur (3*p*) and a combination of silicon (3*s*) and (3*p*) atomic orbitals. This is comparable to the situation in silica polymorphs where the top of the valence band is dominated by non-bonding oxygen (2*p*) states and the bottom of the conduction band by silicon (3*s*) and/or (3*p*) states. The above results suggest that while the band gap narrows considerably upon replacing O with S, its qualitative chemical nature remains the same. On comparing the composition of the valence band in tetragonal SiS_2 and SiO_2 cristobalite, we further note that the contribution of silicon states is considerably larger in the sulphide, suggesting a more covalent material. This result is consistent with Wannier analysis data (see below).

3.4. Bonding properties

Linear combination of atomic orbitals considerations suggest that each S (or O) atom in SiX_2 materials is bonded to the central

Table 6
Results of the Wannier analysis for the valence orbitals in SiS_2 and SiO_2 structures

	P	σ (Å)	Σ
Tetragonal SiS_2	0.22	1.11	0.51–0.52
Orthorhombic SiS_2	0.22–0.23	1.10	0.51
SiS_2 quartz	0.23–0.24	1.12–1.13	0.52–0.53
SiO_2 cristobalite	0.49–0.52	0.74	0.46
SiO_2 quartz	0.50–0.52	0.74–0.75	0.46

The symbols P, σ and Σ are defined in the text.

Si-atom by a single σ valence molecular orbital completely filled with an electron pair, a picture that is supported by an analysis of the localized Wannier functions, obtained from a Boys localization of the electron density [47,48]. A comparison of bonding Si–X Wannier functions in SiO_2 cristobalite and tetragonal SiS_2 is given in Fig. 7. For each SiS_2 material studied, the Wannier functions corresponding to the Si–S valence molecular orbitals are centred along the Si–S direction, and have contributions from both the Si and S atoms, while the molecular orbitals' centres of charge are shifted away from the middle of the bond towards the more electronegative S atom. The magnitude of this shift is defined by the polarization fraction (P) [48], which indicates how far the centre of charge projected on the bond axis for a valence electron pair (projected valence electron centre of charge, PVECC) is shifted away from the bond's midpoint ($P = 0$ is the covalent limiting case with the PVECC lying exactly in the middle of the bond, while $P = 1$ is the ionic limiting case with the charge centred on the most electronegative atom in the bond). Table 6 shows that the polarization fraction P of the PBE/LGTO optimized sulphide materials is much smaller than in the two SiO_2 materials considered. This feature is also evident in Fig. 7, where we can clearly observe the higher contribution of O than S to Si–X bonding Wannier functions. This observation, which is in line with an earlier study on quartz-structured materials [42], suggests that bonding in the silicon sulphide compounds has a considerably more covalent character than in silica. A similar conclusion can be drawn from a comparison of the spatial spread of the bonding Wannier functions (σ), which is a measure of their spatial extent. The spatial spread of the bonding Wannier functions in the sulphides is consistently larger than for their silica analogs, although this may be partly due to the more diffuse 3s and 3p states on the sulphur. However, if we correct for this to a first order by scaling the spatial spread by the Si–X bond length (Σ as introduced in [48]) the effect remains. Increasing the basis-set is found to have no discernable effect on these conclusions. The bonding electrons in the sulphide appear thus to be less strongly bound than in silica and more delocalized over the length of the bond, again suggesting a more covalent character of the Si–S bond, and most likely explaining the increased flexibility of tetrahedral TX_2 sulphides.

4. Conclusions

The energetics, structure and physical properties of tetragonal and orthorhombic SiS_2 have been studied by periodic (hybrid) density functional theory. Our calculations show that the experimental crystal structures are generally well reproduced, but that calculations using localized orbitals require a sizable basis-set in order to reproduce geometries obtained with projected augmented wave bases at the same level of theory. The basis-set requirement is more stringent for sulphides than for oxides, due to the presence of softer degrees of freedom in the potential energy surface. The best match between experimental and calculated crystal structures is obtained with the hybrid PBE0 functional. Relative energies of different crystal structures, in contrast, are found to be similar for calculations involving the PBE and PBE0 density functionals and virtually independent on the basis used. The energy landscape of SiS_2 is dramatically different from that of silica. More specifically, orthorhombic SiS_2 which consists of 1D chains of edge-sharing tetrahedra held together by van der Waals interactions is the lowest energy SiS_2 structure in our study, while its silica analog (just as all silica materials with edge-sharing tetrahedra) is known from previous calculations to lie much higher in energy than corner-sharing silica polymorphs such as quartz and cristobalite. This clear change in the energetic preference of assembling the SiX_2 tetrahedra in space is accompanied by a considerable decrease in the size of the Si–X–Si angles and a broadening of the Si–X–Si angle distribution. Other effects of the substitution of sulphur for oxygen include an overall increase of the flexibility of the material (as probed by vibrational frequencies) and a considerable narrowing of the Kohn–Sham band gap. The latter is in line with the experimental observation of photoluminescence in the related $GaGeS_2$ compounds and suggests that tetragonal SiS_2, which has an almost direct band gap, might find application in near UV light emitting diodes. The narrowing of the band gap finally causes an increase of the static and high-frequency dielectric tensors in sulphides, as well as a more covalent character of Si–S bonds compared to Si–O in silica, as further confirmed by analysis of the maximally localized Wannier orbitals.

Acknowledgments

We kindly acknowledge Drs. B. Slater, G. Tribello, A.A. Sokol and Prof. S.T. Bromley for stimulating discussion. M.A.Z. acknowledges the European Commission for a Marie Curie Intra-European Fellowship (MEIF-CT-2005-010326).

References

[1] M. O'Keeffe, G.V. Gibbs, J. Phys. Chem. 89 (1985) 4574–4577.
[2] J.A. Tossell, Chem. Mater. 6 (1994) 239–248.
[3] Y. Tukoda, T. Uchino, T. Yoko, J. Non-Cryst. Solids 282 (2001) 256–264.
[4] S. Blaineau, P. Jund, D. Drabold, Phys. Rev. B. 67 (2003) 094204.
[5] S. Blaineau, P. Jund, Phys. Rev. B 70 (2004) 184210.
[6] B.T. Kolomiets, Phys. Status Solidi 7 (1964) 359–372.
[7] S.R. Ovshinsky, Phys. Rev. Lett. 21 (1968) 1450–1453.
[8] A. Yoshikawa, O. Ochi, H. Nagai, Y. Mizushima, Appl. Phys. Lett. 31 (1977) 161–163.
[9] N.F. Zheng, X.H. Bu, B. Wang, P.Y. Feng, Science 298 (2002) 2366–2369.
[10] A. Weiss, A. Weiss, Z. Anorg. Allg. Chem. 276 (1954) 95–112.
[11] H. Gabriel, C. Alvarez-Totstado, J. Am. Chem. Soc. 74 (1952) 262–264.
[12] I. Tomaszkiewicz, G.A. Hope, O.A.G. O'Hare, J. Chem. Thermodyn. 29 (1997) 1031–1045.
[13] J. Peters, B. Krebs, Acta Crystallogr. B 38 (1982) 1270–1272.
[14] S.I. Troyanov, Zh. Neorg. Khim. 45 (2000) 1619–1624.
[15] M.S. Silverman, J.R. Soulen, Inorg. Chem. 4 (1965) 129–130.
[16] C.T. Prewitt, H.S. Young, Science 149 (1965) 535–537.
[17] G.A. Berzovskii, L.E. Gorsh, I.E. Paukov, Russ. J. Phys. Chem. 53 (1979) 1704–1705.
[18] J.P. Perdew, K. Burke, M. Ernzerhof, Phys. Rev. Lett. (1996) 773865–773868.
[19] J.P. Perdew, M. Emzerhof, K. Burke, J. Chem. Phys. 105 (1996) 9982–9985.
[20] R. Dovesi, V.R. Saunders, C. Roetti, R. Orlando, C.M. Zicovich-Wilson, F. Pascale, B. Civalleri, K. Doll, N.M. Harrison, I.J. Bush, Ph.D' . Arco, M. Llunell, CRYSTAL06 User's Manual, Universita' di Torino, Torino, 2006.
[21] C.M. Zicovich-Wilson, R. Dovesi, J. Mol. Catal. A: Chemical 119 (1997) 449–458.
[22] M. Catti, Phys. Rev. B 65 (2002) 224115.
[23] D.E. Woon, T.H. Dunning, J. Chem. Phys. 98 (1993) 1358–1371.
[24] F. Pascale, C.M. Zicovich-Wilson, F. Lopez Gejo, B. Civalleri, R. Orlando, R. Dovesi, J. Comput. Chem. 25 (2004) 888–897.
[25] C.M. Zicovich-Wilson, F. Pascale, C. Roetti, V.R. Saunders, R. Orlando, R. Dovesi, J. Comput. Chem. 25 (2004) 1873–1881.
[26] C. Darringan, M. Rerat, G. Malia, R. Dovesi, J. Comp. Chem. 24 (2003) 1305–1312.
[27] P.E. Blöchl, Phys. Rev. B 50 (1994) 17953–17979.

[28] G. Kresse, D. Joubert, Phys. Rev. B 59 (1999) 1758–1775.
[29] G. Kresse, J. Hafner, Phys. Rev. B 47 (1993) 558–561.
[30] P.M. Piccione, C. Laberty, S.Y. Yang, M.A. Camblor, A. Navrotsky, M.E. Davis, J. Phys. Chem. B 104 (2000) 10001–10011.
[31] N.J. Henson, A.K. Cheetham, J.D. Gale, Chem. Mater. 6 (1994) 1647–1650.
[32] B. Civalleri, C.M. Zicovich-Wilson, P. Ugliengo, V.R. Saunders, R. Dovesi, Chem. Phys. Lett. 292 (1998) 394–402.
[33] M. Catti, B. Civalleri, P. Ugliengo, J. Phys. Chem. B 104 (2000) 7259–7265.
[34] R. Astala, S.M. Auerbach, P.A. Monson, J. Phys. Chem. B 108 (2004) 9208.
[35] M.A. Zwijnenburg, F. Corà, R.G. Bell, J. Phys. Chem. B 111 (2007) 6156–6160.
[36] M.A. Zwijnenburg, F. Corà, R.G. Bell, J. Am. Chem. Soc. 129 (2007) 12588.
[37] D.R. Hamann, Phys. Rev. B 55 (1997) 14784–15793.
[38] D.R. Hamann, Phys. Rev. B 73 (2006) 219903(E).
[39] S.T. Bromley, I.P.R. Moreira, F. Illas, J.C. Wojdel, Phys. Rev. B 73 (2006) 134202.
[40] S.T. Bromley, M.A. Zwijnenburg, T. Maschmeyer, Phys. Rev. Lett. 90 (2003) 035502.
[41] S.T. Bromley, Nano Lett. 4 (2004) 1427–1432.
[42] M.A. Zwijnenburg, R. Huenerbein, R.G. Bell, F. Corá, J. Solid State Chem. 179 (2006) 3429–3436.
[43] I.P. Swainson, M.T. Dove, Phys. Rev. Lett. 71 (1993) 193–196.
[44] E.A. Mikajlo, H.E. Dorsett, M.J. Ford, J. Chem. Phys. 120 (2004) 10799–10806.
[45] K. Tanaka, M. Yamaguchi, J. Non-Cryst. Solids 230 (1998) 757–760.
[46] I. Vurgaftman, J.R. Meyer, L.R. Ram-Mohan, J. Appl. Phys. 89 (2001) 5815.
[47] C.M. Zicovich-Wilson, R. Dovesi, V.R Saunders, J. Chem. Phys. 115 (2001) 9708–9719.
[48] C.M. Zicovich-Wilson, A. Bert, C. Roetti, R. Dovesi, V.R. Saunders, J. Chem. Phys. 116 (2002) 1120–1127.